Article

Hybrid TSR–PSR Alternate Energy Harvesting Relay Network over Rician Fading Channels: Outage Probability and SER Analysis

Tan N. Nguyen [1], Phu Tran Tin [1] ID, Duy Hung Ha [1], Miroslav Voznak [1] ID, Phuong T. Tran [2,*], Minh Tran [3] and Thanh-Long Nguyen [4]

[1] VSB-Technical University of Ostrava 17. listopadu 15/2172, 708 33 Ostrava-Poruba, Czech Republic; nguyennhattan@tdtu.edu.vn (T.N.N.); phutrantin@iuh.edu.vn (P.T.T.); haduyhung@tdtu.edu.vn (D.H.H.); miroslav.voznak@vsb.cz (M.V.)
[2] Wireless Communications Research Group, Faculty of Electrical and Electronics Engineering, Ton Duc Thang University, Ho Chi Minh City, Vietnam
[3] Optoelectronics Research Group, Faculty of Electrical and Electronics Engineering, Ton Duc Thang University, Ho Chi Minh City, Vietnam; tranhoangquangminh@tdtu.edu.vn
[4] Center for Information Technology, Ho Chi Minh City University of Food Industry, Ho Chi Minh City, Vietnam; longthng@gmail.com
* Correspondence: tranthanhphuong@tdtu.edu.vn; Tel.: +84-283-775-5028

Abstract: In this research, we investigate a hybrid time-switching relay (TSR)–power-splitting relay (PSR) alternate energy harvesting (EH) relaying network over the Rician fading channels. For this purpose, the amplify-and-forward (AF) mode is considered for the alternative hybrid time TSR–PSR. The system model consists of one source, one destination and two alternative relays for signal transmission from the source to the destination. In the first step, the exact and asymptotic expressions of the outage probability and the symbol errors ratio (SER) are derived. Then, the influence of all system parameters on the system performance is investigated, and the Monte Carlo simulation verifies all results. Finally, the system performances of TSR–PSR, TSR, and PSR cases are compared in connection with all system parameters.

Keywords: half-duplex; amplify-and-forward (AF); outage probability; TSR–PSR; SER

1. Introduction

Currently, energy harvesting (EH) from green environmental sources and the conversion of this energy into the electrical energy used to supply communication network devices is considered to be a leading research direction. Furthermore, this solution can provide not only environmentally friendly energy supplies, but also self-maintained, long-lived, and autonomous communication systems. In the series of primary environmentally green energy sources, such as solar, wind, geothermal, and mechanical energy, radio frequency (RF) signals can be considered as a prospective energy source in the future. The RF sources can be used independently from time and location in urban areas and can be produced cheaply in small dimensions, which could be a significant advantage in the manufacturing of small and low-cost communication devices such as sensor nodes. Moreover, RF signals could provisionally fill the role of information transmission or energy harvesting in the sensor nodes. Wireless power transfer and the harvesting of electrical energy from a power source to one or more electrical loads is a well-known technique in communication networks. Thus, this research direction for RF-powered mobile networks has received significant attention during the last decade in wireless sensor networks (WSNs) and cooperative communication systems from both academia

and industry [1–9]. Furthermore, EH wireless communication can substantially prolong the network lifetime for wireless sensor networks with low power nodes, and RF signals can recharge nodes more controllably. Wireless nodes can harvest RF energy either in the time domain before data reception, or in the power domain by dividing the received RF signals for the EH and information decoding (ID) [9–12]. In a cooperative network, references [13–16] developed two new relaying protocols based on the receiver structures adopted at R, termed time-switching-based relaying (TSR) and power-splitting-based relaying (PSR). From [14–16], the TSR and PSR protocols have some drawbacks; for instance, TSR loses information in the switching process to the harvesting mode, and PSR has a low coverage area. Furthermore, PSR requires a complicated hardware structure to make sure that a proper portion of energy from the source signal is extracted for energy harvesting. In contrast, TSR can simplify the hardware at the expense of the throughput or achievable rate of the system. Based on the fact that both TSR and PSR protocols have their drawbacks, the proposed method combines these two protocols to get the best out of them. This solution is obtained in this paper by using an adaptive relaying protocol [17,18]. From the other point of view, the authors highlighted the problem of maximizing the throughput in connection with power allocation and the degree of channel state information (CSI) in [19], and secrecy systems operating over spatially correlated composite fading channels are presented in [20]. Also, the performance of dynamic relays in different types of cellular networks under the presence of inter-cell interference (ICI) is investigated in [21], and a novel approach for maintaining the gains of relaying and keeping the signaling overheads at a low level is proposed in [22]. Furthermore, maximizing harvested power in MIMO SWIPT systems with PSR is investigated in [23], the joint design of spatial channel assignment and power allocation in MIMO systems is studied in [24], and ref. [25] considers a dual-hop cognitive inter-vehicular relay-assisted communication system by the double Rayleigh fading distribution.

The main objective of this paper is to provide a system performance analysis (in terms of the outage probability and symbol error ratio (SER)) of hybrid TSR–PSR alternate energy harvesting relaying networks over Rician fading channels. In the analysis process, we analyze and derive the exact and asymptotic expressions of the outage probability and SER. After that, the Monte Carlo simulation is used to validate the analytical analysis in connection with all system parameters. The main contributions of this research are as follows:

(1) We propose and investigate the alternative hybrid TSR–PSR energy harvesting relaying networks over Rician fading channels. In this model, two relays R1 and R2 are alternatively used for energy harvesting and data transmission process from S to D;

(2) The exact and asymptotic expressions of the outage probability and SER are proposed, analyzed and derived. Moreover, the comparison of the exact and asymptotic expressions of the outage probability and SER in three cases—TSR, PSR, and TSR–PSR—is demonstrated;

(3) The influence of all system parameters on the outage probability and SER is investigated and discussed;

(4) The Monte Carlo simulation is used to verify all the research results.

The rest of this manuscript is organized as follows. In Section 2, we present the proposed system model. Section 3 investigates the exact and asymptotic analysis of the outage probability and SER. Numerical results and a discussion are given in Section 4. Section 5 concludes this manuscript.

2. System Model

Consider an AF relaying system with four nodes: the source S, two relays R_1, R_2 and the destination D as shown in Figure 1. Each device works with a single antenna and in a half-duplex (HD) mode, and there is no direct link between R and D. In this model, S, and D have their own stable power supplies, while R1 and R2 operate with EH and alternately forward source data according to the AF protocol. We denote that h_1 and h_2 are the fading channel gains from the source to relays, g_1 and g_2 are the fading channel gain from the relays R_1 and R_2 to the destination D, and h_{12} and h_{21} are the gain factors between R_1 and R_2, respectively [26–29].
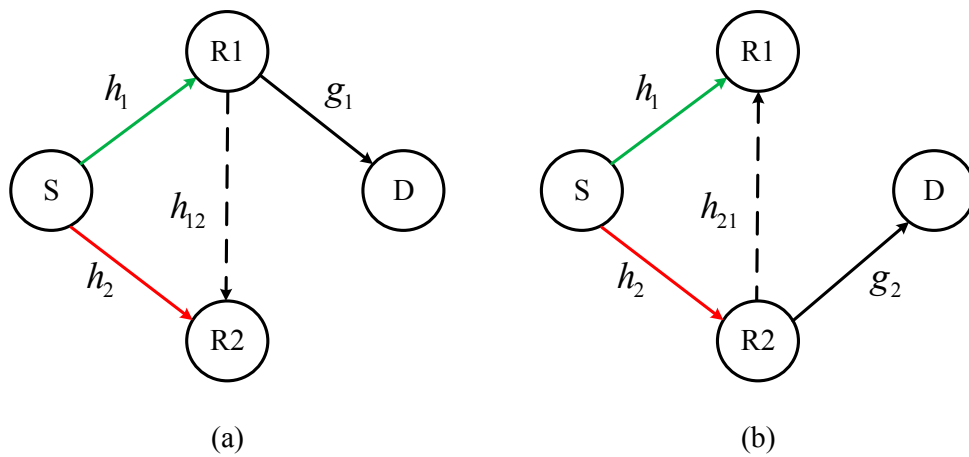
Figure 1. The system model. The green, red and black lines represent the first-hop and second-hop transmission, respectively. The green and dashed back lines represent the data transmission (DT) and energy harvesting (EH), respectively. (**a**) R_1-DT and R_2-EH; (**b**) R_2-DT and R_1-EH.

Moreover, Figure 2 shows the division of the transmission time. In the first interval time αT with $0 \leq \alpha < 1$, S transfers energy by signal to R_1 and R_2. After that, S transfers the part of energy ρP_s ($0 \leq \rho < 1$) to R_1 in the next $(1-\alpha)T/2$ interval time and uses $(1-\rho)P_s$ energy to transfer information to R_1. In the same interval time, R_2 harvests energy from S. In the final $(1-\alpha)T/2$ interval time, R_1 transfers information to D and R_2 harvests energy from R_1 [14,25,26,29].

In this model, R_1 forwards the source information data to D by using its energy harvested in the current T blocks and the previous T blocks. Please note that R_1 and R_2 always harvest energy from the received RF signals in all of the first T blocks. In the following T blocks, R_2 works as a helping relay, while R_1 harvests energy in all T blocks by overhearing the transmissions from S and R_2. The EH and data relay of R_2 are performed similarly to the above procedure for R_1. Thus, R_1 and R_2 will alternately forward source data in every T block. Compared with the TS-EH or PS-EH-based single-relay system, more energy can be harvested by relays in our protocol for the DT [14,26,29].
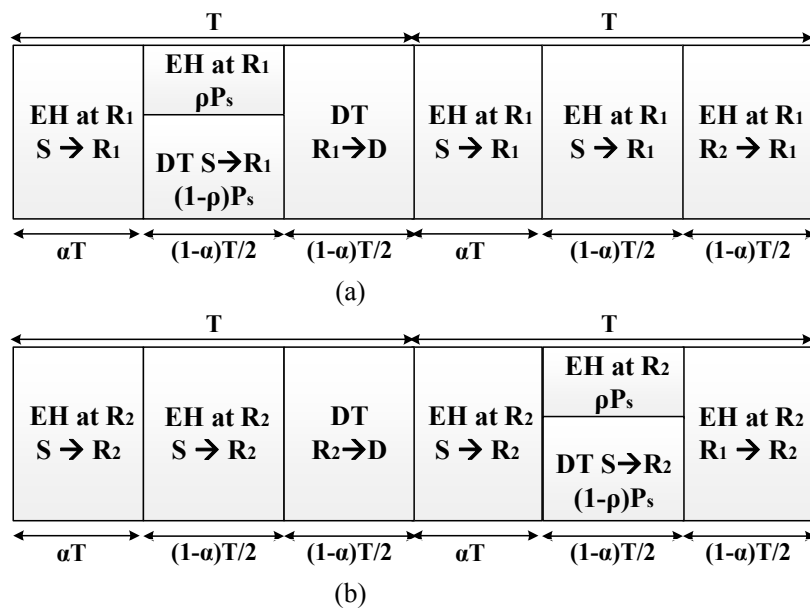
EH: Energy Harvesting   DT: Data Transmission

Figure 2. The information transmission and energy harvesting process. (**a**) R_1-DT and R_2-EH; (**b**) R_2-DT and R_1-EH.

3. System Performance

In this section, we analyze and investigate the energy harvesting and data transmission processes in the two relays in the hybrid TSR–PSR protocol. To increase the understanding of the readers, we show all symbols used in Table 1.

Table 1. All symbols used.

Symbol	Definition
$0 < \eta < 1$	Energy conversion efficiency
$0 \leq \alpha < 1$	Time-switching factor
$0 \leq \rho < 1$	Power-splitting factor
P_s/N_0	Source-power-to-noise ratio
K	Rician K-factor
λ_1	Mean of $|h_1|^2$
λ_2	Mean of $|g_1|^2$
R	Source rate
E_{r1}	Harvested energy at relay 1
P_{r1}	Average transmit power of relay 1
E_{r2}	Harvested energy at relay 2
P_{r2}	Average transmit power of relay 2
P_{out}	Outage probability
γ_{e2e1}	End to end signal to noise ratio
$K_v(\bullet)$	Modified Bessel function of the second kind and vth order
$\Gamma(\bullet)$	Gamma function
$F(v, \beta; \gamma; z)$	Hypergeometric function
SER	Symbol error ratio
β	Amplifying factor
$Q(t)$	Gaussian Q-function
P_s	Transmit power of the source
T	Total time of processing

In the system model, the inter-relay channel is assumed to be symmetric, i.e., $h_{12} = h_{21}$. Rician block fading is assumed, so all the channels are circularly-symmetric jointly-Gaussian complex random and denoted as $h_i \approx C(0,1)$, $g_i \approx C(0,1)$ and $h_{12} \approx C(0,1)$, where $i \in (1,2)$.

In the hybrid TSR–PSR alternative relaying, the source provides an energy signal to both R_1 and R_2 in αT and $(1-\alpha)T/2$ blocks. In the $(1-\alpha)T/2$ block, R_1 allocates $0 \leq \rho < 1$ (ρ is the power splitting factor) as part of the received source signal for the energy harvesting (EH). Therefore, the total harvested energy at R_1 can be given by

$$E_{r1a} = \eta \alpha T P_s + \frac{\eta \rho (1-\alpha) T P_s}{2} \tag{1}$$

where $(E\left\{|h_i|^2\right\} = 1$ and $h_i \approx C(0,1)$, $g_i \approx C(0,1)$, $h_{12} \approx C(0,1))$, $0 < \eta < 1$ and $0 \leq \alpha < 1$ are the energy conversion efficiency and time-switching factor, respectively.

In this model, the average EH amount by omitting the small-scale channel fading is proposed and considered.

In a similar way, the total harvested energy at R_2 can be given by the equation below:

$$E_{r2a} = \eta \alpha T P_s + \frac{\eta \rho (1-\alpha) T P_s}{2} \tag{2}$$

When S provides the data to R_1, after splitting the ρ part of the received signal for the EH at the relays, the remaining signal at R_1 can be obtained as

$$y_{r1} = \sqrt{1-\rho}h_1 x_s + n_{r1} \tag{3}$$

where n_{r1} is the additive white Gaussian noise (AWGN) with variance N_0 at R_1, and $E\left\{|x_s|^2\right\} = P_s$ in which $E\{\bullet\}$ is expectation operator.

Furthermore, R_1 amplifies and forwards the signal to D in the next stage. The transmitted signal from R_1 can be expressed as

$$x_{r1} = \beta y_{r1} \tag{4}$$

where $\beta = \dfrac{\sqrt{P_{r1}}}{\sqrt{(1-\rho)P_s|h_1|^2 + N_0}}$ is the amplifying factor.

Then, the received signal at D can be formulated as the following expression:

$$y_{1d} = g_1 x_{r1} + n_{1d} \tag{5}$$

where n_{1d} is the additive white Gaussian noise (AWGN) with variance N_0 at D, $E\left\{|x_{r1}|^2\right\} = P_{r1}$, and P_{r1} is the average transmitted power of R_1.

Replacing (3) and (4) into (5), the received signal at D can be obtained as:

$$y_{1d} = \beta g_1 \left[\sqrt{1-\rho}h_1 x_s + n_{r1}\right] + n_{1d} = \underbrace{\beta g_1 \sqrt{1-\rho}h_1 x_s}_{signal} + \underbrace{\beta g_1 n_{r1} + n_{1d}}_{noise} \tag{6}$$

In this case, when R_1 performs the delay-tolerant (DT) transmission mode, the end to end signal to noise ratio (SNR) at D can be calculated as

$$\gamma_{e2e1} = \frac{E\left\{|signal|^2\right\}}{E\left\{|noise|^2\right\}} = \frac{\beta^2 |g_1|^2 |h_1|^2 P_s (1-\rho)}{\beta^2 |g_1|^2 N_0 + N_0} \tag{7}$$

After algebra calculation and using the fact that $N_0 << P_r$, the end to end SNR can be obtained:

$$\gamma_{e2e1} = \frac{(1-\rho)P_s P_{r1}|h_1|^2|g_1|^2}{|g_1|^2 N_0 + (1-\rho)P_s|h_1|^2 N_0} \tag{8}$$

In this T block time, R_2 can harvest energy from S in $\alpha T + (1-\alpha)T/2$ blocks, i.e., $\frac{T}{2}(1+\alpha)$ blocks, and R_2 can also harvest energy from R_1 in $(1-\alpha)T/2$ blocks. Therefore, the total harvested energy at R_2 when R_1 joins in the data transmission (DT) can be calculated by

$$E_{r2b} = \frac{\eta(1+\alpha)TP_s}{2} + \frac{\eta(1-\alpha)TP_{r1}}{2} \tag{9}$$

Similar to R_2, the total harvested energy at R_1 when R_2 joins in the DT can be obtained as

$$E_{r1b} = \frac{\eta(1+\alpha)TP_s}{2} + \frac{\eta(1-\alpha)TP_{r2}}{2} \tag{10}$$

where P_{r2} is the average transmitted power of R_2.

From the EH process at R_1 in the previous T blocks and current T blocks, the total harvested energy of R_1 for DT can be obtained as

$$\begin{aligned}
E_{r1} &= E_{r1a} + E_{r1b} = \eta\alpha TP_s + \frac{\eta\rho(1-\alpha)TP_s}{2} + \frac{\eta(1+\alpha)TP_s}{2} + \frac{\eta(1-\alpha)TP_{r2}}{2} \\
&= \frac{\eta T[(3\alpha - \alpha\rho + 1)P_s + \rho + (1-\alpha)P_{r2}]}{2}
\end{aligned} \tag{11}$$

because of the symmetry property in our proposed system. Similar to R_1, the total harvested energy of R_2 also can be obtained as the following:

$$E_{r2} = E_{r2a} + E_{r2b} = \frac{\eta T[(3\alpha - \alpha\rho + 1)P_s + \rho + (1 - \alpha)P_{r1}]}{2} \tag{12}$$

From (11), the average transmitted power of R_1 can be calculated as

$$P_{r1} = \frac{E_{r1}}{(1-\alpha)T/2} = \frac{\eta T[(3\alpha - \alpha\rho + 1)P_s + \rho + (1 - \alpha)P_{r2}]}{(1-\alpha)T} = \eta \left[\frac{(3\alpha - \alpha\rho + 1)P_s + \rho}{1 - \alpha} + P_{r2} \right] \tag{13}$$

From (12), the average transmitted power of R_2 also can be obtained as

$$P_{r2} = \frac{E_{r2}}{(1-\alpha)T/2} = \eta \left[\frac{(3\alpha - \alpha\rho + 1)P_s + \rho}{1 - \alpha} + P_{r1} \right] \tag{14}$$

Substituting (14) into (13), we obtain

$$P_{r1} = \frac{\eta \Psi}{1 - \eta} \tag{15}$$

where we denote $\Psi = \frac{(3\alpha - \alpha\rho + 1)P_s + \rho}{1 - \alpha}$.

Finally, the SNR of the proposed system in (7) can be rewritten as the following:

$$\gamma_{e2e1} = \frac{(1-\rho)P_s P_{r1}|h_1|^2|g_1|^2}{|g_1|^2 N_0 + (1-\rho)P_s|h_1|^2 N_0} = \frac{(1-\rho)P_s P_{r1}\varphi_1\varphi_2}{\varphi_2 N_0 + (1-\rho)P_s\varphi_1 N_0} \tag{16}$$

where $\varphi_1 = |h_1|^2$, $\varphi_2 = |g_1|^2$ and P_{r1} is defined by (15).

3.1. Exact Outage Probability Analysis

The probability density function (PDF) of random variable (RV) φ_i (where i = 1, 2) as in [28] is

$$f_{\varphi_i}(x) = a \sum_{l=0}^{\infty} \frac{(bK)^l}{(l!)^2} x^l e^{-bx} \tag{17}$$

where we denote $\varphi_1 = |h_1|^2$, $\varphi_2 = |g_1|^2$, $a = \frac{(K+1)e^{-K}}{\lambda_i}$, $b = \frac{K+1}{\lambda_i}$, in which λ_i is the unit mean value of RV φ_i where i = 1, 2, respectively, because we consider the small-scale power fading $|h_1|^2$, $|g_1|^2$ in the derivation. Therefore, a and b can be re-denoted as $a = (K+1)e^{-K}$, $b = K+1$, K is the Rician K-factor defined as the ratio of the power of the line-of-sight (LOS) component to the scattered components.

The cumulative density function (CDF) of RV φ_i, where i = 1, 2, can be computed as in [17]:

$$F_{\varphi_i}(\varsigma) = \int_0^{\varsigma} f_{\varphi_i}(x)dx = 1 - \frac{a}{b} \sum_{l=0}^{\infty} \sum_{n=0}^{l} \frac{K^l b^n}{l!n!} \varsigma^n e^{-b\varsigma} = 1 - \sum_{l=0}^{\infty} \sum_{n=0}^{l} \frac{K^l b^n e^{-K}}{l!n!} \varsigma^n e^{-b\varsigma} \tag{18}$$

$$F_{\varphi_i}(\varsigma) = \int_0^{\varsigma} f_{\varphi_i}(x)dx = 1 - \frac{a}{b} \sum_{l=0}^{\infty} \sum_{n=0}^{l} \frac{K^l b^n}{l!n!} \varsigma^n e^{-b\varsigma} = 1 - \sum_{l=0}^{\infty} \sum_{n=0}^{l} \frac{K^l b^n e^{-K}}{l!n!} \varsigma^n e^{-b\varsigma} \tag{19}$$

Theorem 1 (Exact Outage Probability)**.** *The expression of the exact outage probability of the proposed system can be formulated by the following:*

$$P_{out}^1 = 1 - 2ae^{-K}e^{-\frac{b\gamma_{th}N_0}{P_{r1}P_s(1-\rho)}}e^{-\frac{b\gamma_{th}N_0}{P_{r1}}}\sum_{l=0}^{\infty}\sum_{m=0}^{\infty}\sum_{n=0}^{l}\sum_{k=0}^{n+m}\frac{K^{l+m}b^{n+m}(\gamma_{th}N_0)^{n+m+1}(n+m)!}{l!(m!)^2 n!k!(n+m-k)!P_{r1}{}^{n+m+1}[P_s(1-\rho)]^{\frac{2n+m-k+1}{2}}}$$
$$\times K_{m-k+1}\left(\frac{2b\gamma_{th}N_0}{P_{r1}\sqrt{P_s(1-\rho)}}\right) \tag{20}$$

where $K_v(\bullet)$ is the modified Bessel function of the second kind and vth order.

Proof of Theorem 1. See Appendix A. □

3.2. Asymptotic Outage Probability Analysis

From (16), at the high SNR regime, the end to end SNR can be approximated as

$$\gamma_{\gamma_{e2e1}}^{\infty} = \frac{(1-\rho)P_s P_{r1}\varphi_1\varphi_2}{\varphi_2 N_0 + (1-\rho)P_s\varphi_1 N_0} \approx \frac{P_{r1}\varphi_2}{N_0} \tag{21}$$

Then, the asymptotic outage probability can be formulated as

$$P_{out}^{1,\infty} = \Pr\left(\frac{P_{r1}\varphi_2}{N_0} < \gamma_{th}\right) = \Pr\left(\varphi_2 < \frac{\gamma_{th}N_0}{P_{r1}}\right) = 1 - \sum_{l=0}^{\infty}\sum_{n=0}^{l}\frac{K^l b^n e^{-K}}{l!n!}\left(\frac{\gamma_{th}N_0}{P_{r1}}\right)^n e^{-\frac{b\gamma_{th}N_0}{P_{r1}}} \tag{22}$$

3.3. SER (Symbol Error Ratio) Analysis

In this section, we obtain new expressions for the symbol error ratio (SER) at the destination. We first consider the outage probability, which was obtained in [30,31]. Thus, we obtain

$$SER_1 = E\left[\phi Q\sqrt{2\theta\gamma_{e2e1}}\right] \tag{23}$$

$Q(t) = \frac{1}{\sqrt{2\pi}}\int_t^{\infty}e^{-x^2/2}dx$ is the Gaussian Q-function, ω and θ are constants which are specific for the modulation type. $(\phi,\theta) = (1,1)$ for BPSK and $(\phi,\theta) = (1,2)$ for QPSK. For this purpose, the distribution function of γ_{e2e1} is considered for analyzing the SER performance. Then, Equation (22) can be rewritten directly regarding the outage probability at the source by using integration as follows:

$$SER_1 = \frac{\phi\sqrt{\theta}}{2\sqrt{\pi}}\int_0^{\infty}\frac{e^{-\theta x}}{\sqrt{x}}F_{\gamma_{e2e1}}(x)dx \tag{24}$$

Theorem 2 (Exact SER). *The exact SER can be calculated by the below expression:*

$$SER_1 = \frac{\phi}{2} - ae^{-K}\phi\sqrt{\theta}\sum_{l=0}^{\infty}\sum_{m=0}^{\infty}\sum_{n=0}^{l}\sum_{k=0}^{n+m}\frac{4^{m-k+1}K^{l+m}b^{n+2m-k+1}(n+m)!(N_0)^{n+2m-k+2}}{l!(m!)^2 n!k!(n+m-k)!P_{r1}{}^{n+2m-k+2}[P_s(1-\rho)]^{\frac{2n+3m-3k+3}{2}}}$$
$$\times\frac{1}{\left[\theta+\frac{3bN_0}{P_{r1}\sqrt{P_s(1-\rho)}}+\frac{bN_0}{P_{r1}}\right]^{n+2m-k+5/2}}\times\frac{\Gamma\left(n+2m-k+\frac{5}{2}\right)\Gamma\left(n+k+\frac{1}{2}\right)}{\Gamma(n+m+2)}$$
$$\times F\left(n+2m-k+\frac{5}{2},m-k+\frac{3}{2};n+m+2;\frac{\theta-\frac{bN_0}{P_{r1}\sqrt{P_s(1-\rho)}}+\frac{bN_0}{P_{r1}}}{\theta+\frac{3bN_0}{P_{r1}\sqrt{P_s(1-\rho)}}+\frac{bN_0}{P_{r1}}}\right) \tag{25}$$

where $\Gamma(\bullet)$ is the gamma function, and $F(v,\beta;\gamma;z)$ is a hypergeometric function.

Proof of Theorem 2. See Appendix B. □

Theorem 3 (Asymptotic SER Analysis). *The asymptotic SER can be formulated by the below equation:*

$$SER_1^\infty = \frac{\phi}{2} - \frac{e^{-K}\phi\sqrt{\theta}}{2\sqrt{\pi}} \sum_{l=0}^{\infty} \sum_{n=0}^{l} \frac{K^l b^n}{l!n!} \left(\frac{N_0}{P_{r1}}\right)^n \left(\theta + \frac{bN_0}{P_{r1}}\right)^{-n-1/2} \Gamma\left(n + \frac{1}{2}\right) \tag{26}$$

Proof of Theorem 3. See Appendix C.　□

4. Numerical Results and Discussion

For validation of the correctness of the derived outage probability and SER expressions, as well as the investigation of the effect of various parameters on the system performance, a set of Monte Carlo simulations are conducted and presented in this section. For each simulation, we first provide the graphs of the outage probability and SER obtained by the analytical formulas. Secondly, we plot the same outage probability and SER curves that result from the Monte Carlo simulation. To do this, we generate 10^6 random samples of each channel gain, which are Rician distributed. The analytical curve and the simulation curve should match to verify the correctness of our analysis. All simulation parameters are listed in Table 2.

Table 2. Simulation parameters.

Symbol	Values
$0 < \eta \leq 1$	0.7
λ_1	1
λ_2	1
P_s/N_0	0:20 dB
K	3
R	0.5 bps

Figure 3 shows the outage probability of the model system versus η in three cases—TSR, PSR, TSR–PSR. In this model, we set P_s/N_0 = 10 dB, ρ = 0.5 and α = 0.5. From the results, we see that the outage probability decreases remarkably while η varies from 0 to 1. The research results show that the numerical results and simulation results match exactly with each other, validating the correctness of the theoretical analysis in the above section. Furthermore, the function of the outage probability to K is presented in Figure 4. Similarly, we set P_s/N_0 = 10 dB, ρ = 0.5 and α = 0.5, and the outage probability decreases remarkably while K varies from 0 to 4. Once again, the simulation results and theoretical results agree well with each other.

Figure 5 plots the numerical and simulation results of the system outage probability in connection with the ratio P_s/N_0. In Figure 5, both the exact and asymptotic outage probability in cases TSR, PSR, and TSR–PSR are illustrated. The main parameters are set as R = 0.5, ρ = 0.3 and α = 0.3. From the results, the exact outage probability decreases and comes close to the asymptotic line when the ratio P_s/N_0 increases from 0 to 20 dB. On another hand, the influence of R on the outage probability in three cases—TSR, PSR, TSR–PSR—is investigated in Figure 6 with P_s/N_0 = 15 dB, ρ = 0.7 and α = 0.3. The outage probability significantly increases with R from 0 to 4. From Figures 5 and 6, the analytical results and the simulation results match well with each other for all values of R and P_s/N_0.

Figure 7 illustrates the numerical and simulation results of the system outage probability concerning α and ρ with P_s/N_0 = 10 dB. It is clearly shown that the outage probability increases with increasing α and ρ, and the minimum outage probability can be obtained with α = 0 and ρ = 1. Moreover, SER versus the ratio P_s/N_0 in three cases—TSR, PSR, and TSR–PSR—is shown in Figure 8. Furthermore, Figure 9 plots the comparison of the exact and asymptotic outage probability of three cases—TSR, PSR, and TSR–PSR—versus P_s/N_0. The results indicate that all the simulation and analytical values agreed well with each other.
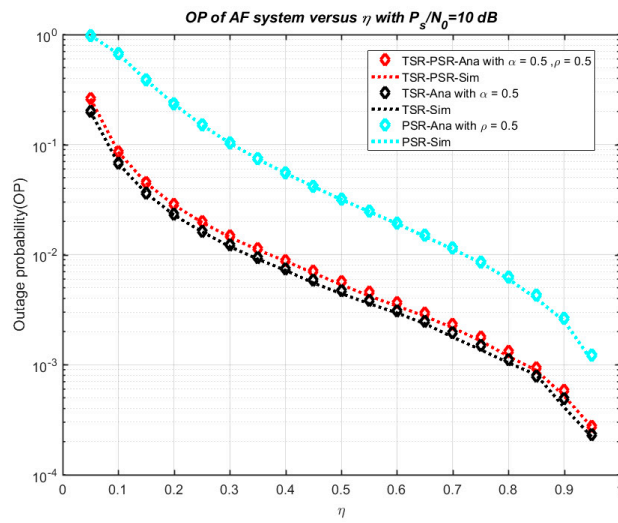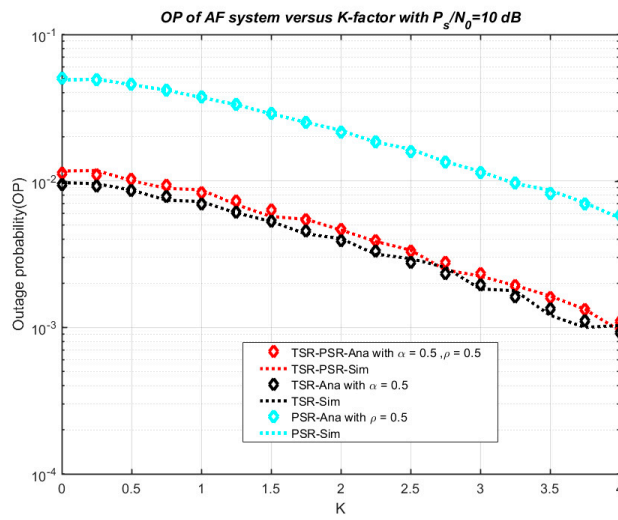
Figure 3. Outage probability versus η.

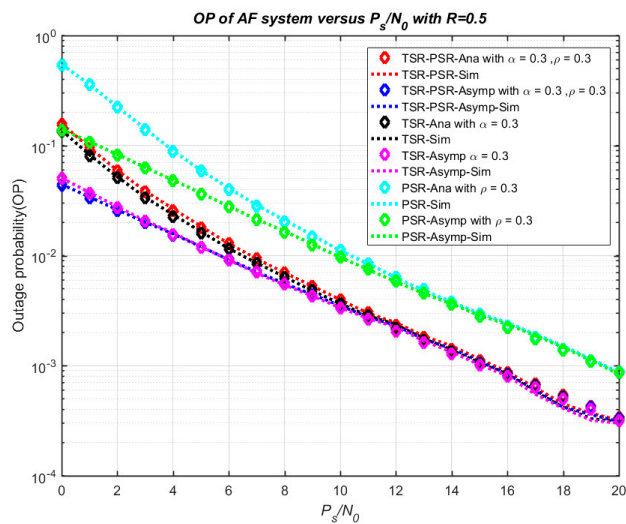**Figure 4.** Outage probability versus K.
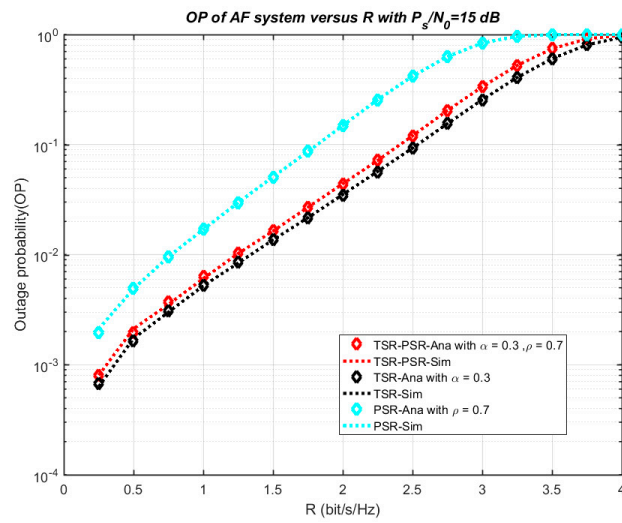

Figure 5. Outage probability versus P_s/N_0.

Figure 6. Outage probability versus R.

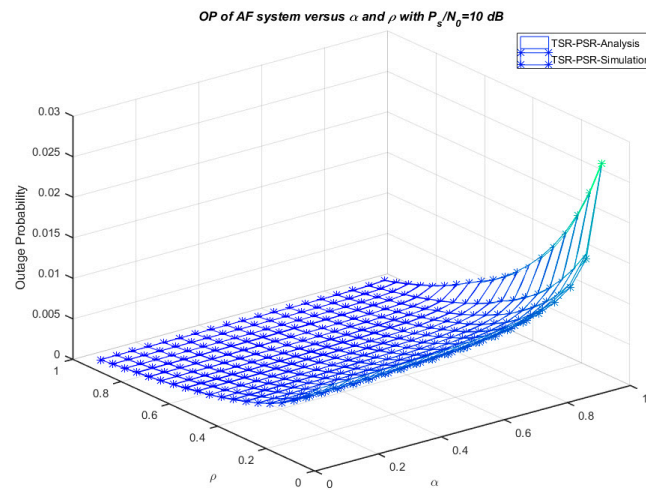**Figure 7.** Outage probability versus ρ and α.
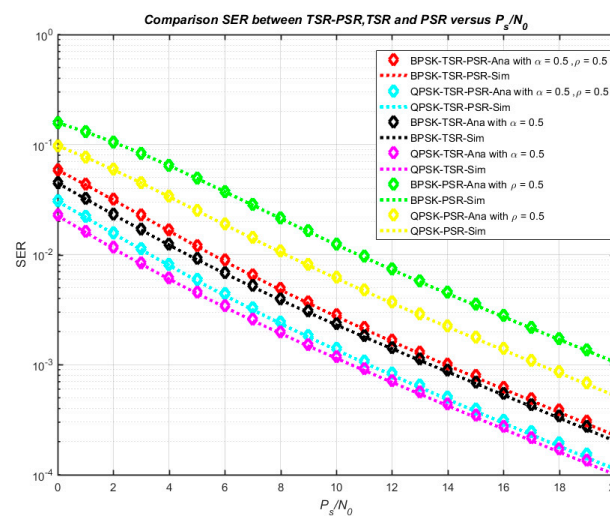

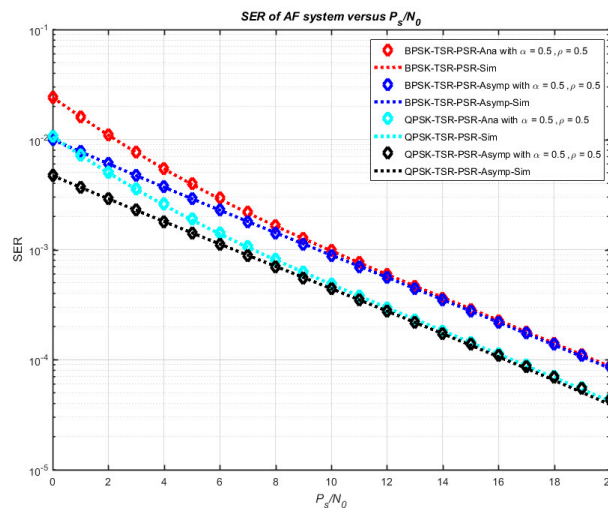**Figure 8.** SER versus P_s/N_0 in the cases TSR, PSR, and TSR–PSR.

Figure 9. The exact and asymptotic SER versus P_s/N_0.

5. Conclusions

In this research, the hybrid TSR–PSR alternate EH relay network over AF-based Rician fading channels is presented and investigated. The system model consists of one source, one destination and two alternative relays for signal transmission from the source to the destination. We derive the exact and asymptotic expressions of the outage probability and SER and investigate the influence of all system parameters on the system performance using the Monte Carlo simulation. The research results indicate that the alternative hybrid TSR–PSR has better performance in comparison with the TSR and PSR cases. The research results can provide essential recommendations for communication network research and practice directions.

Appendix A. Proof of Theorem 1—Exact Outage Probability

The outage probability of the model system can be calculated as

$$P_{out}^1 = \Pr(\gamma_{e2e1} < \gamma_{th}) = \Pr\left[\frac{(1-\rho)P_s P_{r1}\varphi_1\varphi_2}{\varphi_2 N_0 + (1-\rho)P_s\varphi_1 N_0} < \gamma_{th}\right] = \Pr[(1-\rho)P_s\varphi_1\{P_{r1}\varphi_2 - \gamma_{th}N_0\} < \gamma_{th}\varphi_2 N_0] \tag{A1}$$

$$P_{out}^1 = \Pr\begin{cases} \varphi_1 < \frac{\gamma_{th}\varphi_2 N_0}{P_s(1-\rho)[P_{r1}\varphi_2 - \gamma_{th}N_0]} &, \varphi_2 > \frac{\gamma_{th}N_0}{P_{r1}} \\ 1 &, \varphi_2 \leq \frac{\gamma_{th}N_0}{P_{r1}} \end{cases} \tag{A2}$$

where $\gamma_{th} = 2^{2R} - 1$ is threshold and R is the source rate.

The Equation (A2) can be rewritten as

$$P_{out}^1 = \int_0^{\frac{\gamma_{th}N_0}{P_{r1}}} f_{\varphi_2}(\varphi_2)d\varphi_2 + \int_{\frac{\gamma_{th}N_0}{P_{r1}}}^{\infty} F_{\varphi_1}\left\{\frac{\gamma_{th}\varphi_2 N_0}{P_s(1-\rho)[P_{r1}\varphi_2 - \gamma_{th}N_0]}|\varphi_2\right\}f_{\varphi_2}(\varphi_2)d\varphi_2 \tag{A3}$$

From (18), the outage probability can be formulated as the following

$$
\begin{aligned}
P_{out}^1 = & \int_0^{\frac{\gamma_{th} N_0}{P_{r1}}} f_{\varphi_2}(\varphi_2) d\varphi_2 + \\
& \int_{\frac{\gamma_{th} N_0}{P_{r1}}}^{\infty} \left\{ 1 - \sum_{l=0}^{\infty} \sum_{n=0}^{l} \frac{K^l b^n e^{-K}}{l! n!} \left(\frac{\gamma_{th} \varphi_2 N_0}{P_s(1-\rho)[P_{r1}\varphi_2 - \gamma_{th} N_0]} \right)^n e^{-b\left(\frac{\gamma_{th} \varphi_2 N_0}{P_s(1-\rho)[P_{r1}\varphi_2 - \gamma_{th} N_0]} \right)} \right\} f_{\varphi_2}(\varphi_2) d\varphi_2
\end{aligned}
\tag{A4}
$$

$$
P_{out}^1 = 1 - \int_{\frac{\gamma_{th} N_0}{P_{r1}}}^{\infty} \left\{ \sum_{l=0}^{\infty} \sum_{n=0}^{l} \frac{K^l b^n e^{-K}}{l! n!} \left(\frac{\gamma_{th} \varphi_2 N_0}{P_s(1-\rho)[P_{r1}\varphi_2 - \gamma_{th} N_0]} \right)^n e^{-b\left(\frac{\gamma_{th} \varphi_2 N_0}{P_s(1-\rho)[P_{r1}\varphi_2 - \gamma_{th} N_0]} \right)} \right\} f_{\varphi_2}(\varphi_2) d\varphi_2
\tag{A5}
$$

Furthermore, from (17) we obtain

$$
P_{out}^1 = 1 - \int_{\frac{\gamma_{th} N_0}{P_{r1}}}^{\infty} \left\{ \sum_{l=0}^{\infty} \sum_{n=0}^{l} \frac{K^l b^n e^{-K}}{l! n!} \left(\frac{\gamma_{th} \varphi_2 N_0}{P_s(1-\rho)[P_{r1}\varphi_2 - \gamma_{th} N_0]} \right)^n e^{-b\left(\frac{\gamma_{th} \varphi_2 N_0}{P_s(1-\rho)[P_{r1}\varphi_2 - \gamma_{th} N_0]} \right)} \right\} a \sum_{l=0}^{\infty} \frac{(bK)^l}{(l!)^2} x^l e^{-bx} d\varphi_2
\tag{A6}
$$

$$
P_{out}^1 = 1 - \int_{\frac{\gamma_{th} N_0}{P_{r1}}}^{\infty} a e^{-K} \sum_{l=0}^{\infty} \sum_{m=0}^{\infty} \sum_{n=0}^{l} \frac{K^{l+m} b^{n+m}}{l!(m!)^2 n!} \left(\frac{\gamma_{th} \varphi_2 N_0}{P_s(1-\rho)[P_{r1}\varphi_2 - \gamma_{th} N_0]} \right)^n e^{-b\left(\frac{\gamma_{th} \varphi_2 N_0}{P_s(1-\rho)[P_{r1}\varphi_2 - \gamma_{th} N_0]} \right)} \varphi_2^m e^{-b\varphi_2} d\varphi_2
\tag{A7}
$$

By changing a variable $t = P_{r1}\varphi_2 - \gamma_{th} N_0$ in to (25), we obtain

$$
P_{out}^1 = 1 - \frac{a e^{-K}}{P_{r1}} \int_0^{\infty} \sum_{l=0}^{\infty} \sum_{m=0}^{\infty} \sum_{n=0}^{l} \frac{K^{l+m} b^{n+m}}{l!(m!)^2 n!} \left(\frac{\gamma_{th} \left[\frac{t+\gamma_{th} N_0}{P_{r1}} \right] N_0}{P_s(1-\rho)t} \right)^n e^{-b\left(\frac{\gamma_{th} \left[\frac{t+\gamma_{th} N_0}{P_{r1}} \right] N_0}{P_s(1-\rho)t} \right)} \left[\frac{t+\gamma_{th} N_0}{P_{r1}} \right]^m e^{-b\left[\frac{t+\gamma_{th} N_0}{P_{r1}} \right]} dt
\tag{A8}
$$

$$
P_{out}^1 = 1 - \frac{a e^{-K} e^{-\frac{b\gamma_{th} N_0}{P_{r1} P_s(1-\rho)}} e^{-\frac{b\gamma_{th} N_0}{P_{r1}}}}{P_{r1}} \int_0^{\infty} \sum_{l=0}^{\infty} \sum_{m=0}^{\infty} \sum_{n=0}^{l} \frac{K^{l+m} b^{n+m}}{l!(m!)^2 n! P_{r1}^{n+m}} \left[\frac{\gamma_{th} N_0}{P_s(1-\rho)} \right]^n t^{-n} e^{-\frac{b\gamma_{th}^2 N_0^2}{P_{r1} P_s(1-\rho)t}} [t+\gamma_{th} N_0]^{n+m} e^{-\frac{bt}{P_{r1}}} dt
\tag{A9}
$$

Now, by applying the equation $(x+y)^n = \sum_{k=0}^{n} \begin{pmatrix} n \\ k \end{pmatrix} x^{n-k} y^k$ to (20), the outage probability can be demonstrated as follows:

$$
\begin{aligned}
P_{out}^1 = & 1 - \frac{a e^{-K} e^{-\frac{b\gamma_{th} N_0}{P_{r1} P_s(1-\rho)}} e^{-\frac{b\gamma_{th} N_0}{P_{r1}}}}{P_{r1}} \sum_{l=0}^{\infty} \sum_{m=0}^{\infty} \sum_{n=0}^{l} \sum_{k=0}^{n+m} \frac{K^{l+m} b^{n+m} (n+m)! (\gamma_{th} N_0)^{n+k}}{l!(m!)^2 n! k! (n+m-k)! P_{r1}^{n+m}} \left[\frac{1}{P_s(1-\rho)} \right]^n \\
& \times \int_0^{\infty} t^{m-k} e^{-\frac{b\gamma_{th}^2 N_0^2}{P_{r1} P_s(1-\rho)t}} e^{-\frac{bt}{P_{r1}}} dt
\end{aligned}
\tag{A10}
$$

Apply (3.471,9) of [32]:

$$
\begin{aligned}
P_{out}^1 = & 1 - \frac{2 a e^{-K} e^{-\frac{b\gamma_{th} N_0}{P_{r1} P_s(1-\rho)}} e^{-\frac{b\gamma_{th} N_0}{P_{r1}}}}{P_{r1}} \sum_{l=0}^{\infty} \sum_{m=0}^{\infty} \sum_{n=0}^{l} \sum_{k=0}^{n+m} \frac{K^{l+m} b^{n+m} (\gamma_{th} N_0)^{n+k} (n+m)!}{l!(m!)^2 n! k! (n+m-k)! P_{r1}^{n+m} [P_s(1-\rho)]^n} \\
& \times \left(\frac{\gamma_{th}^2 N_0^2}{P_s(1-\rho)} \right)^{\frac{m-k+1}{2}} \times K_{m-k+1} \left(\frac{2b\gamma_{th} N_0}{P_{r1}\sqrt{P_s(1-\rho)}} \right)
\end{aligned}
\tag{A11}
$$

Appendix B. Proof of Theorem 2—Exact SER Analysis

Substituting (17) into (26):

$$
SER_1 = \frac{\phi\sqrt{\theta}}{2\sqrt{\pi}} \int_0^{\infty} \frac{e^{-\theta x}}{\sqrt{x}} \left\{ \begin{array}{l} 1 - 2 a e^{-K} \sum_{l=0}^{\infty} \sum_{m=0}^{\infty} \sum_{n=0}^{l} \sum_{k=0}^{n+m} \frac{K^{l+m} b^{n+m} (n+m)!}{l!(m!)^2 n! k! (n+m-k)! P_{r1}^{n+m+1} [P_s(1-\rho)]^{\frac{2n+m-k+1}{2}}} \\ \times (x N_0)^{n+m+1} \times e^{-\frac{bx N_0}{P_{r1} P_s(1-\rho)}} \times e^{-\frac{bx N_0}{P_{r1}}} \times K_{m-k+1} \left(\frac{2bx N_0}{P_{r1}\sqrt{P_s(1-\rho)}} \right) \end{array} \right\} dx
\tag{A12}
$$

From (A12), we obtain:

$$I_1 = \frac{\phi\sqrt{\theta}}{2\sqrt{\pi}} \int\limits_0^\infty \frac{e^{-\theta x}}{\sqrt{x}} dx \tag{A13}$$

and

$$
\begin{aligned}
I_2 &= \frac{ae^{-K}\phi\sqrt{\theta}}{\sqrt{\pi}} \sum_{l=0}^\infty \sum_{m=0}^\infty \sum_{n=0}^l \sum_{k=0}^{n+m} \frac{K^{l+m}b^{n+m}(n+m)!(N_0)^{n+m+1}}{l!(m!)^2 n!k!(n+m-k)!P_{r1}^{n+m+1}[P_s(1-\rho)]^{\frac{2n+m-k+1}{2}}} \\
&\quad \times \int\limits_0^\infty (x)^{n+m+1} \times \frac{e^{-\theta x}}{\sqrt{x}} \times e^{-\frac{bxN_0}{P_{r1}P_s(1-\rho)}} \times e^{-\frac{bxN_0}{P_{r1}}} \times K_{m-k+1}\left(\frac{2bxN_0}{P_{r1}\sqrt{P_s(1-\rho)}}\right) dx
\end{aligned}
\tag{A14}
$$

Firstly, we consider $I_1 = \frac{\phi\sqrt{\theta}}{2\sqrt{\pi}} \int\limits_0^\infty \frac{e^{-\theta x}}{\sqrt{x}} dx$.

We use the table of integral Equation (3.361,1) in [32]:

$$I_1 = \frac{\phi\sqrt{\theta}}{2\sqrt{\pi}} \times \frac{\sqrt{\pi}}{\sqrt{\theta}} = \frac{\phi}{2} \tag{A15}$$

We consider

$$
\begin{aligned}
I_2 &= \frac{ae^{-K}\phi\sqrt{\theta}}{\sqrt{\pi}} \sum_{l=0}^\infty \sum_{m=0}^\infty \sum_{n=0}^l \sum_{k=0}^{n+m} \frac{K^{l+m}b^{n+m}(n+m)!(N_0)^{n+m+1}}{l!(m!)^2 n!k!(n+m-k)!P_{r1}^{n+m+1}[P_s(1-\rho)]^{\frac{2n+m-k+1}{2}}} \\
&\quad \times \int\limits_0^\infty x^{n+m+1/2} \times e^{-x\left[\theta+\frac{bN_0}{P_{r1}P_s(1-\rho)}+\frac{bN_0}{P_{r1}}\right]} \times K_{m-k+1}\left(\frac{2bxN_0}{P_{r1}\sqrt{P_s(1-\rho)}}\right) dx
\end{aligned}
\tag{A16}
$$

$$J_1 = \int\limits_0^\infty x^{n+m+1/2} \times e^{-x\left[\theta+\frac{bN_0}{P_{r1}P_s(1-\rho)}+\frac{bN_0}{P_{r1}}\right]} \times K_{m-k+1}\left(\frac{2bxN_0}{P_{r1}\sqrt{P_s(1-\rho)}}\right) dx \tag{A17}$$

We use the table of integral Equation (6.621,3) in [32]:

$$
\begin{aligned}
J_1 &= \frac{\sqrt{\pi}\left[\frac{4bN_0}{P_{r1}\sqrt{P_s(1-\rho)}}\right]^{m-k+1}}{\left[\theta+\frac{3bN_0}{P_{r1}\sqrt{P_s(1-\rho)}}+\frac{bN_0}{P_{r1}}\right]^{n+2m-k+5/2}} \times \frac{\Gamma\left(n+2m-k+\frac{5}{2}\right)\Gamma\left(n+k+\frac{1}{2}\right)}{\Gamma(n+m+2)} \\
&\quad \times F\left(n+2m-k+\frac{5}{2}, m-k+\frac{3}{2}; n+m+2; \frac{\theta-\frac{bN_0}{P_{r1}\sqrt{P_s(1-\rho)}}+\frac{bN_0}{P_{r1}}}{\theta+\frac{3bN_0}{P_{r1}\sqrt{P_s(1-\rho)}}+\frac{bN_0}{P_{r1}}}\right)
\end{aligned}
\tag{A18}
$$

where $\Gamma(\bullet)$ is the gamma function, and $F(v, \beta; \gamma; z)$ is a hypergeometric function.

Then:

$$
\begin{aligned}
I_2 &= \frac{ae^{-K}\phi\sqrt{\theta}}{\sqrt{\pi}} \sum_{l=0}^\infty \sum_{m=0}^\infty \sum_{n=0}^l \sum_{k=0}^{n+m} \frac{K^{l+m}b^{n+m}(n+m)!(N_0)^{n+m+1}}{l!(m!)^2 n!k!(n+m-k)!P_{r1}^{n+m+1}[P_s(1-\rho)]^{\frac{2n+m-k+1}{2}}} \\
&\quad \times \frac{\sqrt{\pi}\left[\frac{4bN_0}{P_{r1}\sqrt{P_s(1-\rho)}}\right]^{m-k+1}}{\left[\theta+\frac{3bN_0}{P_{r1}\sqrt{P_s(1-\rho)}}+\frac{bN_0}{P_{r1}}\right]^{n+2m-k+5/2}} \times \frac{\Gamma\left(n+2m-k+\frac{5}{2}\right)\Gamma\left(n+k+\frac{1}{2}\right)}{\Gamma(n+m+2)} \\
&\quad \times F\left(n+2m-k+\frac{5}{2}, m-k+\frac{3}{2}; n+m+2; \frac{\theta-\frac{bN_0}{P_{r1}\sqrt{P_s(1-\rho)}}+\frac{bN_0}{P_{r1}}}{\theta+\frac{3bN_0}{P_{r1}\sqrt{P_s(1-\rho)}}+\frac{bN_0}{P_{r1}}}\right)
\end{aligned}
\tag{A19}
$$

$$
\begin{aligned}
I_2 &= ae^{-K}\phi\sqrt{\theta} \sum_{l=0}^\infty \sum_{m=0}^\infty \sum_{n=0}^l \sum_{k=0}^{n+m} \frac{4^{m-k+1}K^{l+m}b^{n+2m-k+1}(n+m)!(N_0)^{n+2m-k+2}}{l!(m!)^2 n!k!(n+m-k)!P_{r1}^{n+2m-k+2}[P_s(1-\rho)]^{\frac{2n+3m-3k+3}{2}}} \\
&\quad \times \frac{1}{\theta\left[\phi+\frac{3bN_0}{P_{r1}\sqrt{P_s(1-\rho)}}+\frac{bN_0}{P_{r1}}\right]^{n+2m-k+5/2}} \times \frac{\Gamma\left(n+2m-k+\frac{5}{2}\right)\Gamma\left(n+k+\frac{1}{2}\right)}{\Gamma(n+m+2)} \\
&\quad \times F\left(n+2m-k+\frac{5}{2}, m-k+\frac{3}{2}; n+m+2; \frac{\theta-\frac{bN_0}{P_{r1}\sqrt{P_s(1-\rho)}}+\frac{bN_0}{P_{r1}}}{\theta+\frac{3bN_0}{P_{r1}\sqrt{P_s(1-\rho)}}+\frac{bN_0}{P_{r1}}}\right)
\end{aligned}
\tag{A20}
$$

Appendix C. Proof of Theorem 3—Asymptotic SER Analysis

We obtain

$$
\begin{aligned}
SER_1^\infty &= \frac{\phi\sqrt{\theta}}{2\sqrt{\pi}}\int_0^\infty \frac{e^{-\theta x}}{\sqrt{x}}\left\{1 - \sum_{l=0}^\infty \sum_{n=0}^l \frac{K^l b^n e^{-K}}{l!n!}\left(\frac{xN_0}{P_{r1}}\right)^n e^{-\frac{bxN_0}{P_{r1}}}\right\}dx \\
&= \frac{\phi\sqrt{\theta}}{2\sqrt{\pi}}\int_0^\infty \frac{e^{-\theta x}}{\sqrt{x}}dx - \frac{e^{-K}\phi\sqrt{\theta}}{2\sqrt{\pi}}\sum_{l=0}^\infty \sum_{n=0}^l \frac{K^l b^n}{l!n!}\left(\frac{N_0}{P_{r1}}\right)^n \int_0^\infty x^n \times \frac{e^{-\theta x}}{\sqrt{x}}\times e^{-\frac{bxN_0}{P_{r1}}}dx
\end{aligned}
\tag{A21}
$$

We consider

$$
I_3 = \int_0^\infty x^n \times \frac{e^{-\theta x}}{\sqrt{x}}\times e^{-\frac{bxN_0}{P_{r1}}}dx = \int_0^\infty x^{n-1/2}\times e^{-x\left(\theta+\frac{bN_0}{P_{r1}}\right)}dx
\tag{A22}
$$

We use the table of integral Equation (3.381,4) in [32]:

$$
I_3 = \left(\theta + \frac{bN_0}{P_{r1}}\right)^{-n-1/2}\Gamma\left(n+\frac{1}{2}\right)
\tag{A23}
$$

where $\Gamma(\bullet)$ is the gamma function.

References

1. Bi, S.; Ho, C.K.; Zhang, R. Wireless powered communication: Opportunities and challenges. *IEEE Commun. Mag.* **2015**, *53*, 117–125. [CrossRef]
2. Niyato, D.; Kim, D.I.; Maso, M.; Han, Z. Wireless Powered Communication Networks: Research Directions and Technological Approaches. *IEEE Wirel. Commun.* **2017**, 2–11. [CrossRef]
3. Yu, H.; Lee, H.; Jeon, H. What is 5G? Emerging 5G Mobile Services and Network Requirements. *Sustainability* **2017**, *9*, 1848. [CrossRef]
4. Zhou, X.; Zhang, R.; Ho, C.K. Wireless Information and Power Transfer: Architecture Design and Rate-Energy Tradeoff. *IEEE Trans. Commun.* **2013**, *61*, 4754–4767. [CrossRef]
5. Akhtar, R.; Leng, S.; Memon, I.; Ali, M.; Zhang, L. Architecture of Hybrid Mobile Social Networks for Efficient Content Delivery. *Wirel. Pers. Commun.* **2014**, *80*, 85–96. [CrossRef]
6. Rango, F.D.; Gerla, M.; Marano, S. A Scalable Routing Scheme with Group Motion Support in Large and Dense Wireless Ad Hoc Networks. *Comput. Electr. Eng.* **2006**, *32*, 224–240. [CrossRef]
7. Zhou, B.; Lee, Y.; Gerla, M.; de Rango, F. Geo-LANMAR: A Scalable Routing Protocol for Ad Hoc Networks with Group Motion. *Wirel. Commun. Mob. Comput.* **2006**, *6*, 989–1002. [CrossRef]
8. Fazio, P.; de Rango, F.; Sottile, C.; Calafate, C. A New Channel Assignment Scheme for Interference-Aware Routing in Vehicular Networks. In Proceedings of the 2011 IEEE 73rd Vehicular Technology Conference (VTC Spring), Budapest, Hungary, 15–18 May 2011.
9. Cassano, E.; Florio, F.; De Rango, F.; Marano, S. A Performance Comparison between ROC-RSSI and Trilateration Localization Techniques for WPAN Sensor Networks in a Real Outdoor Testbed. In Proceedings of the 2009 Conference on Wireless Telecommunications Symposium, Prague, Czech Republic, 22–24 April 2009.
10. Chen, H.; Zhai, C.; Li, Y.; Vucetic, B. Cooperative Strategies for Wireless-Powered Communications: An Overview. *IEEE Wirel. Commun.* **2018**, *25*, 112–119. [CrossRef]
11. Zhai, C.; Liu, J.; Zheng, L. Relay-Based Spectrum Sharing with Secondary Users Powered by Wireless Energy Harvesting. *IEEE Trans. Commun.* **2016**, *64*, 1875–1887. [CrossRef]
12. Zhai, C.; Zheng, L.; Lan, P.; Chen, H.; Xu, H. Decode-and-forward Two-path Successive Relaying with Wireless Energy Harvesting. In Proceedings of the 2017 IEEE International Conference on Communications Workshops (ICC Workshops), Paris, France, 21–25 May 2017.
13. Chen, Y.; Shi, R.; Feng, W.; Ge, N. AF Relaying with Energy Harvesting Source and Relay. *IEEE Trans. Veh. Technol.* **2016**, *1*. [CrossRef]
14. Zheng, L.; Zhai, C.; Liu, J. Alternate Energy Harvesting and Information Relaying in Cooperative AF Networks. *Telecommun. Syst.* **2017**, *68*, 523–533. [CrossRef]

15. Abbas, H.; Hamdi, K. Millimeter Wave Communications over Relay Networks. In Proceedings of the 2017 IEEE Wireless Communications and Networking Conference (WCNC), San Francisco, CA, USA, 19–22 March 2017.

16. Kong, L.; Khan, M.K.; Wu, F.; Chen, G.; Zeng, P. Millimeter-Wave Wireless Communications for IoT-Cloud Supported Autonomous Vehicles: Overview, Design, and Challenges. *IEEE Commun. Mag.* **2017**, *55*, 62–68. [CrossRef]

17. Zhou, Z.; Peng, M.; Zhao, Z.; Li, Y. Joint Power Splitting and Antenna Selection in Energy Harvesting Relay Channels. *IEEE Signal Process. Lett.* **2015**, *22*, 823–827. [CrossRef]

18. Liu, L.; Zhang, R.; Chua, K. Wireless Information and Power Transfer: A Dynamic Power Splitting Approach. *IEEE Trans. Commun.* **2013**, *61*, 3990–4001. [CrossRef]

19. Zenaidi, M.R.; Rezki, Z.; Tembine, H.; Alouini, M.-S. Performance Limits of Energy Harvesting Communications under Imperfect Channel State Information. In Proceedings of the 2016 IEEE International Conference on Communications (ICC), Kuala Lumpur, Malaysia, 23–27 May 2016.

20. Alexandropoulos, G.C.; Peppas, K.P. Secrecy Outage Analysis Over Correlated Composite Nakagami-m/Gamma Fading Channels. *IEEE Commun. Lett.* **2018**, *22*, 77–80. [CrossRef]

21. Papadogiannis, A.; Alexandropoulos, G.C. System Level Performance Evaluation of Dynamic Relays in Cellular Networks over Nakagami-m Fading Channels. In Proceedings of the 2009 IEEE 20th International Symposium on Personal, Indoor and Mobile Radio Communications, Tokyo, Japan, 13–16 September 2009.

22. Papadogiannis, A.; Alexandropoulos, G.C.; Burr, A.; Grace, D. Bringing Mobile Relays for Wireless Access Networks into Practice–learning When to Relay. *IET Commun.* **2012**, *6*, 618. [CrossRef]

23. Mishra, D.; George, C. Alexandropoulos. Transmit Precoding and Receive Power Splitting for Harvested Power Maximization in MIMO SWIPT Systems. *IEEE Trans. Green Commun. Netw.* **2018**, *2*, 774–786. [CrossRef]

24. Mishra, D.; George, C. Alexandropoulos. Jointly Optimal Spatial Channel Assignment and Power Allocation for MIMO SWIPT Systems. *IEEE Wirel. Commun. Lett.* **2018**, *7*, 214–217. [CrossRef]

25. Duy, T.T.; Son, V.N.; Tung, V.T.; Alexandropoulos, G.C.; Duong, T.Q. Outage Performance of Cognitive Cooperative Networks with Relay Selection over Double-Rayleigh Fading Channels. *IET Commun.* **2016**, *10*, 57–64. [CrossRef]

26. Bhatnagar, M.R. On the Capacity of Decode-and-Forward Relaying over Rician Fading Channels. *IEEE Commun. Lett.* **2013**, *17*, 1100–1103. [CrossRef]

27. Nguyen, T.; Quang Minh, T.; Tran, P.; Vozňák, M. Energy Harvesting over Rician Fading Channel: A Performance Analysis for Half-Duplex Bidirectional Sensor Networks under Hardware Impairments. *Sensors* **2018**, *18*, 1781. [CrossRef] [PubMed]

28. Nguyen, T.N.; Tran, P.T.; Quang Minh, T.H.; Voznak, M.; Sevcik, L. Two-Way Half Duplex Decode and Forward Relaying Network with Hardware Impairment over Rician Fading Channel: System Performance Analysis. *Elektronika Ir Elektrotechnika* **2018**, *24*. [CrossRef]

29. Nasir, A.A.; Zhou, X.; Durrani, S.; Kennedy, R.A. Relaying Protocols for Wireless Energy Harvesting and Information Processing. *IEEE Trans. Wirel. Commun.* **2013**, *12*, 3622–3636. [CrossRef]

30. Nguyen, T.N.; Duy, T.T.; Luu, G.T.; Tran, P.T.; Vozňák, M. Energy Harvesting-based Spectrum Access with Incremental Cooperation, Relay Selection and Hardware Noises. *Radioengineering* **2017**, *26*, 240–250. [CrossRef]

31. Mckay, M.R.; Grant, A.J.; Collings, I.B. Performance Analysis of MIMO-MRC in Double-Correlated Rayleigh Environments. *IEEE Trans. Commun.* **2007**, *55*, 497–507. [CrossRef]

32. Zwillinger, D. *Table of Integrals, Series, and Products*; Academic Press: Cambridge, MA, USA, 2015. [CrossRef]